Engineering xxx (xxxx) xxx

Contents lists available at ScienceDirect

Engineering

journal homepage: www.elsevier.com/locate/eng

Article

Chemical Resistant Yarn with Hierarchical Core–Shell Structure for Safety Monitoring and Tunable Thermal Management in High-Risk Environments

Duo Xu [a,b,#], Yingcun Liu [a,b,#], Can Ge [a,#], Chong Gao [b], Ze Chen [b], Ziyi Su [b], Haoran Gong [b], Weilin Xu [b,*], Jian Fang [a,*]

[a] College of Textile and Clothing Engineering, Soochow University, Suzhou 215123, China
[b] State Key Laboratory of New Textile Materials and Advanced Processing Technologies, Wuhan Textile University, Wuhan 430200, China

ARTICLE INFO

Article history:
Available online xxxx

Keywords:
Hierarchical core–shell structure
Chemical resistant yarn
Wearable strain sensor
Thermoregulation

ABSTRACT

Chemical resistant textiles are vital for safeguarding humans against chemical hazards in various settings, such as industrial production, chemical accidents, laboratory activities, and road transportation. However, the ideal integration of chemical resistance, thermal and moisture management, and wearer condition monitoring in conventional chemically protective textiles remains challenging. Herein, the design, manufacturing, and use of stretchable hierarchical core–shell yarns (HCSYs) for integrated chemical resistance, moisture regulation, and smart sensing textiles are demonstrated. These yarns contain helically elastic spandex, wrapped silver-plated nylon, and surface-structured polytetrafluoroethylene (PTFE) yarns and are designed and manufactured based on a scalable fabrication process. In addition to their ideal chemical resistance performance, HCSYs can function as multifunctional stretchable electronics for real-time human motion monitoring and as the basic element of intelligent textiles. Furthermore, a desirable dynamic thermoregulation function is achieved by exploiting the fabric structure with stretching modulation. Our HCSYs may provide prospective opportunities for the future development of smart protective textiles with high durability, flexibility, and scalability.

1. Introduction

Chemical protection in high-risk environments is crucial for ensuring human health. Insufficient body protection from leakage or splashing of chemical solutions in laboratory accidents, chemical plant accidents, and workshop incidents can result in direct injuries or even disabilities for numerous personnel [1–3]. Thus, chemical resistant textiles play a vital role in personal protection, essentially ensuring the safety and health of individuals [4,5]. However, chemical resistant textiles for real-time motion detection and ideal personal thermal management in high-risk environments are currently lacking.

Recently, various techniques, such as material compounding [6–9], structure optimization [10–14], and novel manufacturing [15–18], have been applied to enable the sensing of yarns/textiles with excellent durability, high sensitivity and stretchability, and fast response time. Although yarn-based strain sensors have been studied extensively in flexible sensing [19–21], little attention has been paid to their compatibility with chemical resistance for personal protection. Protective films have been applied to sensing clothing using various methods to incorporate efficient sensing and chemical resistance functions into smart textiles. These methods include emulsion dipping, laminating composites, and sputter coating [22–26]. However, the limited air permeability and thermoregulatory properties of these chemical resistant textiles hinder the release of heat when the human body sweats. Consequently, wearers may experience discomfort, reduced working efficiency, and heat-induced fatigue [27–30]. Moreover, the demand for advanced textiles that can offer multifunctional integration and superior performance to meet complex application requirements in extreme environments is high [31,32]. In this regard, advanced smart clothing with chemical resistance, human motion detection, and dynamic thermal management capabilities can protect the human body from chemical hazards, enable operators to make timely judgments regarding potential hazards, and provide

* Corresponding authors.
E-mail addresses: weilin_xu@wtu.edu.cn (W. Xu), jian.fang@suda.edu.cn (J. Fang).
[#] These authors contributed equally to this work.

https://doi.org/10.1016/j.eng.2023.06.018

Please cite this article as: D. Xu, Y. Liu, C. Ge et al., Chemical Resistant Yarn with Hierarchical Core–Shell Structure for Safety Monitoring and Tunable Thermal Management in High-Risk Environments, Engineering, https://doi.org/10.1016/j.eng.2023.06.018

wearers with a tunable thermal management option. However, such clothing has not yet been realized.

Herein, a chemical resistant yarn with hierarchical core–shell structures (HCSYs) was fabricated to integrate chemical-harm protection, perform real-time motion detection, and offer tunable thermal management (Fig. 1) using a continuous and scalable textile engineering process. The HCSYs consist of elastic yarns, wrapped conductive yarns (stretchable sensing layer), and network-covered polytetrafluoroethylene (PTFE) yarns (protective layer). The protective surface of the PTFE layer protects the human body from chemical hazards, given that the composite yarn is stretchable. Changes in electrical signals and thermal dispersion can result from stretching-induced hierarchical structure variations when HCSYs are woven as hierarchical core–shell structured yarn-based textiles (HCSTs), thus achieving functional compatibility of operator vital physiological sign monitoring, human–machine interaction, and user-tunable thermoregulability. Thus, multifunctional HCSTs with flexibility, scalability, and durability offer a promising approach for next-generation smart antichemical protective textiles to protect those working in laboratories, chemical plants, special workshops, and emergency sites

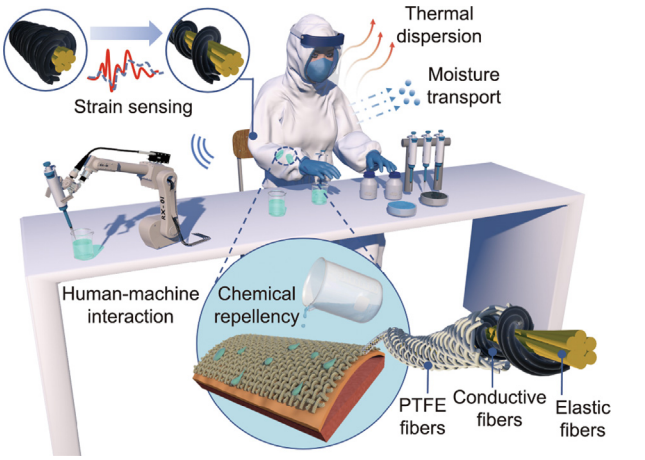

Fig. 1. Schematic and working mechanism of stretchable hierarchical core–shell yarns (HCSYs)/HCSTs. Schematic of the HCSYs/HCSTs with the hierarchical core–shell structure used to integrate the functional application of chemical resistance, real-time motion detection, human–machine interaction, and tunable thermal management in high-risk environments. PTFE: polytetrafluoroethylene.

2. Experimental details

Materials: The silver-plated nylon conductive filaments (280 Denier (D), 18% silver; resistance <40 Ω·m) were purchased from Kazhtex Silver Tech Co. Ltd. (China). The elastic yarn (Spandex, 200 D) was purchased from Hubei Chemical Fiber Co. Ltd. (China). The PTFE (1000 D/3) were purchased from Changzhou Huafu Fluoroplastic Materials Co. Ltd. (China). sodium hydroxide solution (NaOH: 40 wt%) and sulfuric acid solution (H_2SO_4: 99 wt%) were obtained from China National Medicines Co. Ltd. (China). A commercial chemical protective fabric (CCPF) was obtained from a commercial chemical protective suit (CCPS) of Dupont™ Tyvek™ 1422A (USA).

Fabrication of HCSY: The silver-plated nylon conductive yarns of 280 D were produced using a twisting machine with conductive multifilaments. A hollow-spindle fancy twister was used for fabricating wrapped silver-plated nylon/elastic spandex-sensing yarns with a core–sheath structure. Furthermore, the core-sheath-structured sensing yarns were cross-braided by multiple groups of PTFE yarns to form a hierarchical core–shell structure with a modified pre-loading tension.

Fabrication of HCST: The HCST samples were woven using HCSY as weft yarns and PTFE yarns as warp yarns to create a stretching-induced switching structure wrapped with silver-plated nylon/elastic spandex sensing and surface-structured PTFE protective layer domains between the adjoined and separated states, finally forming a hierarchically structured HCST. Subsequently, the HCST piece was integrated with a commercial protective unit under the armpit for a multifunctional demonstration.

Characterizations: The morphologies of the HCSTs were observed using optical microscopy (RH2000; HIROX, Japan). An SL200KS goniometer (KINO Industry Co., Ltd, USA) was used to record the changes in the contact angle of the stretching-induced HCSTs. The tensile properties of the as-prepared samples were analyzed using a universal material testing system (Instron 5943; Instron, USA). Relative resistance changes were measured using a Digital Multimeter (Keysight 34470A; Keysight, USA). A G571 air permeability tester (Standard International Group (HK) Limited, China) was used to test the air permeability of the various textiles with a testing area and pressure of 20 cm^2 and 200 Pa, respectively, according to GB/T 5453 [33].

The water vapor transmission rate of the various textiles was tested using a moisture permeability tester (TS3301; Standard International Group (HK) Limited, China) with the upright cup method, in which the sample size was 25 cm^2, temperature was (38 ± 0.6) °C, and relative humidity was (90% ± 2%) based on American Society of Testing Materials (ASTM) E398 [34]. A thermal constant analyzer (Hot Disk TPS 2500S; Hot Disk AB, Sweden) was used to measure the thermal conductivity using the transient planar heat source method adapted from International Organization for Standardization (ISO) 22007–2 [35]. A thermocouple (HH506RA; Omega, USA) and hygrometer (RHXL5SD; Omega, Switzerland) were used to record the temperature and relative humidity of the artificial skin and human body.

3. Results and discussion

3.1. Fabrication and characterization of HCSYs

Based on the above multifunctional structure design principle, proof-of-concept materials were selected; these include silver-plated nylon, elastic spandex, and PTFE yarns. Silver-plated nylon filament yarn was adopted because of its good electrical conductivity (approximately 40 $\Omega \cdot m^{-1}$) [36], and the PTFE yarn has excellent acid and alkali resistance. Herein, scalable textile engineering techniques (Fig. 2(a)), namely hollow-spindle spinning and braiding, enabled functional selectivity for the continuous manufacturing of our HCSYs by realizing a hierarchical core–shell design. To produce the sensing layer (Fig. S1 in Appendix A), the elastic spandex was consistently guided and fed into the hollow spindle using a tension controller. Subsequently, it was helically wrapped with silver-plated nylon yarns, which had a fineness of 280 D. The wrapping density of the silver-plated nylon yarn was effectively controlled by adjusting the twist level and winding speed. To create HCSYs, PTFE yarns were cross-braided on a tension-controlled helically wrapped sensing layer while the disc rotated in the high-speed braiding machine. The fabrication process of the HCSYs during the operation of the braiding machine can be seen in Movie S1 in Appendix A. Large-scale preparation of HCSYs was achieved, thus allowing continuous winding on cones without any length limitations (Fig. S2 in Appendix A). Owing to this continuous production process, composite yarns of any length can be produced or connected in parallel for wearable electronics, thus enhancing their compatibility with textile processing methods, such as weaving, knitting, and braiding [37].

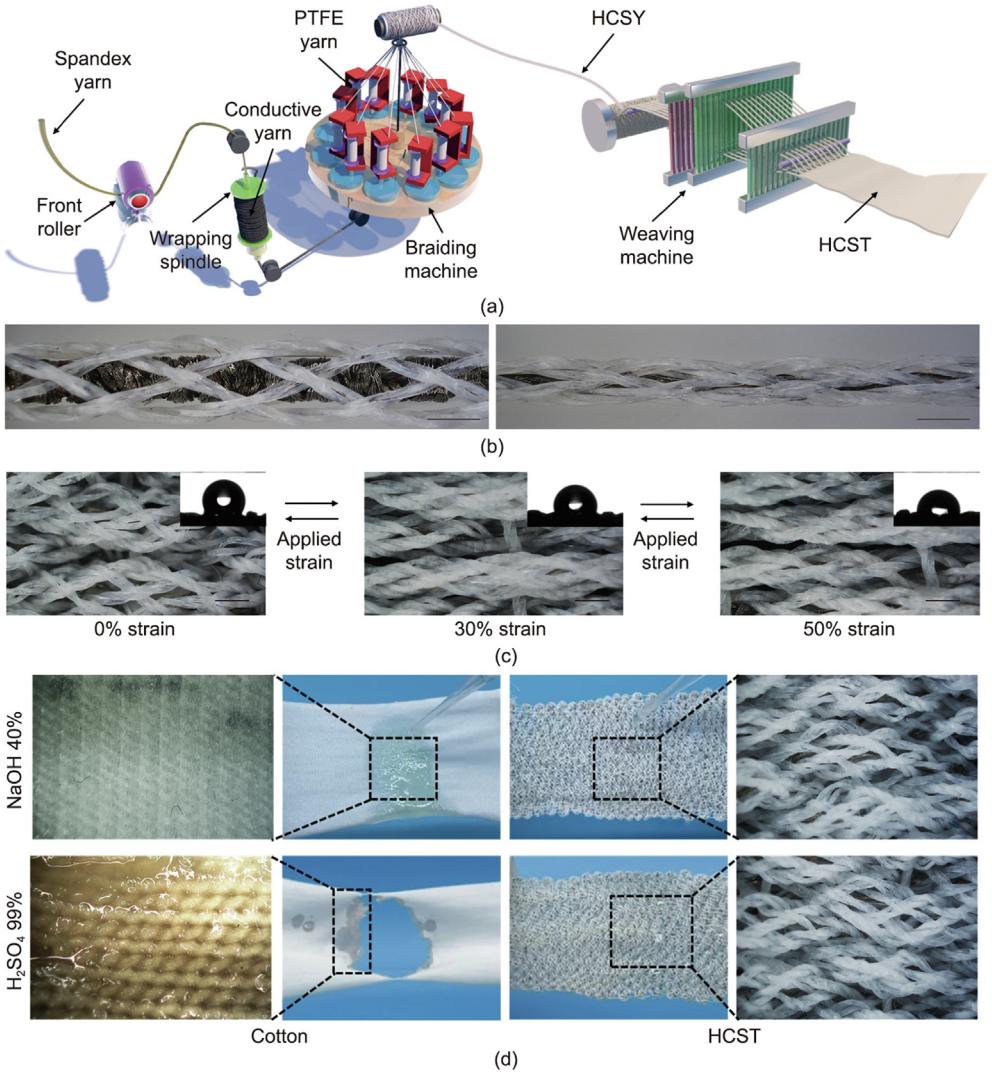

Fig. 2. Fabrication and characterization of HCSYs and HCSTs. (a) Schematic fabrication process of HCSYs and HCSTs. (b) Photograph of as-fabricated HCSYs before (left) and after (right) stretching; scale bars: 1000 μm. (c) Optical images of an HCSTs piece subjected to the applied strains of 0 (left), 30% (middle), and 50% (right). The inserted photographs show the contact angles of a 40 wt% NaOH droplet on HCST; scale bars: 500 μm. (d) Optical photographs showing the chemical resistance of HCSTs (contacted with 40 wt% NaOH (upper); 99 wt% H_2SO_4 (down)); the scale bars in optical images and micrographs are 2 cm and 500 μm, respectively.

The stretching-induced morphology change of the as-fabricated HCSYs is shown in Fig. 2(b), and a cross-sectional photograph of the desired hierarchical core–shell structures is shown Fig. S3 in Appendix A. Tensile testing for the characterization of the representative engineering force versus strain response and typical optical images at different strains obtained for the composite HCSYs are shown in Fig. S4 in Appendix A. Engineering force versus strain curves reveal that HCSYs can readily withstand substantial strain deformation of 50% with a strain force of approximately 0.8 N (±10%). The optical images in Fig. S5 in Appendix A demonstrate the flexibility and stretchability of HCSTs, thus reflecting its excellent wearable performance as a textile. As illustrated in Fig. 2(c) and Fig. S6 in Appendix A, the optical images show that the network-structured PTFE layer on HCSTs surfaces transitioned from a nearly continuous adjoined state to a separated state with gapped domains when stretched along the axis of HCSYs. Further, stable hydrophobicity was endowed by the surface-braided PTFE layer from the slightly changed contact angles (from 108° to 86°) of the chemical droplets on various stretched HCSTs. These aforementioned observations suggest that our HCSTs demonstrates adaptive chemical protection and morphology that can be reconfigured under strain.

3.2. Chemical resistance property of HCSTs

Chemical resistance is critical to ensure safety in high-risk environments. Herein, 10 mL 40 wt% NaOH and 99 wt% H_2SO_4 were dropped on HCSTs and common cotton fabric. Evidently, the cotton fabric gradually disintegrated, whereas the chemical droplets rolled off the surface of the HCSTs, which retained its original appearance and mechanical properties (Fig. 2(d), Figs. S7 and S8, and Movie S2 in Appendix A). When the entire pieces of HCSTs and the cotton fabric were immersed in 40 wt% NaOH and 99 wt % H_2SO_4 solution for 30 min, the cotton was damaged by the NaOH and H_2SO_4 solution, whereas the HCSTs remained in its original state (Fig. S9 in Appendix A). In addition, the chemical droplets still rolled off the surface of the HCSTs at different strain levels up to 50% (Fig. S10 in Appendix A), thus indicating that the hierarchical core–shell structure endows both chemical resistance and stretchability to the HCSTs. The results in Fig. S11 in Appendix A

demonstrate the long-term chemical resistance of the HCSTs, which remains stable even after friction and washing, thus indicating its suitability for prolonged use.

To further verify the chemical performance of the HCSTs, we designed a purpose-made chemical resistance test device consisting of a glass container, test sample, and corrodible material (Fig. 3(a)). Fig. 3(b) shows the test samples covering the corrosive materials for the chemical resistance test, and Fig. 3(c) shows the optical images of the fabric surface when in contact with a 99 wt % H_2SO_4 for 10 min. The cotton fabric immediately exhibited breakage at the contact location with the 99 wt% H_2SO_4; gradually, a large hole formed after 10 min. Further, H_2SO_4 solution spread on the surface of a CCPF. By contrast, the H_2SO_4 droplets concentrated on the surfaces of HCST-0% (0% stain) and HCST-50% (50% stain), thus demonstrating that their surfaces are chemically repellent. Fig. 3(d) shows the chemical-protective performance of the fabrics, in which the corrodible materials covered by the cotton fabrics are completely corroded. Slight corrosion was observed on the corroded material when it was covered with the CCPF. By contrast, the corrodible materials remained in their initial state under the protection of the HCST-0% and HCST-50% samples, thus showing the potential for advanced protective clothing with chemical resistance. This long-term chemical resistance is optimized because the chemical solution can be efficiently blocked from the sensing layer by the network-structured PTFE protective layer, and the functional design of the PTFE protective layer can decrease the gap between the braided PTFE yarns during the stretching process for ideal chemical-harm protection.

3.3. Sensing performance of HCSY

The strain-sensing performance of the HCSY was investigated, and the measurements showed the relative resistance variation ($\Delta R/R_0$) of the yarn samples under various strain-loading conditions. Fig. S12 in Appendix A illustrates the experimental setup diagram for evaluating the electromechanical performance of the HCSY sensors. Evidently, $\Delta R/R_0$ increased with an increase in the wrapping density from 0–4 $T{\cdot}cm^{-1}$, thus suggesting that the HCSY with a wrapping density of 4 $T{\cdot}cm^{-1}$ has a relatively higher sensitivity (Fig. 4(a)). By contrast, a high wrapping density of 5 $T{\cdot}cm^{-1}$ made the helical structure more compact. This explains the smaller resistance change and separation hysteresis resulting from the densely arranged silver-plated nylon yarns. In particular, the $\Delta R/R_0$–strain curve of the aforementioned HCSY exhibited three distinct intervals (strain ranges of: ① 0–5% with a gauge factor (GF) of 5.9, ② 5%–23% with a GF of 3.4, and ③ 23%–50% with a GF of 2.2), as shown in Fig. 4(b). Note that the sensitivity and strain range of the HCSYs are the determining factors for wearable sensors to detect human motion (Table S1 in Appendix A) [38,39]. As shown in Appendix A Fig. S13(a), the hysteresis experiment results revealed that the HCSY sensors exhibited a slight hysteresis of 2.12% at 50% strain, thus indicating excellent stability and reliability of the HCSY sensor for full-range strain–sensing detection. The HCSY sensors exhibited a rapid resistance response within 40 ms (Fig. S13(b) in Appendix A). The inset images in Fig. 4(b) show that the brightness of the light-emitting diode is consistent with the change in resistance of the HCSYs; the smaller the deformation of the HCSYs, the brighter the illuminated light-emitting diode. As shown in Appendix A Figs. S14 and S15, the HCSYs with varied braiding numbers and pitches of PTFE yarns exhibited similar strain-sensing performances before contact with the chemical solution. However, only the HCSY with 16 braided PTFE yarns and a pitch of 24 mm was stably maintained with a slight resistance loss after exposure to H_2SO_4 for 10 min, thus indicating that the HCSY sensors are highly chemically resistant for long-term use.

The change in resistance was attributed to the deformation of the helical conformation of the silver-plated nylon yarn when subjected to tensile strain [40,41]. The resistance variation in the HCSYs can be attributed to the mechanism in which neighboring coils of the silver-plated nylon yarn separate owing to stretching. Consequently, the stretching force disrupts the conductive pathway between the twisted staple fibers, thereby leading to a decrease in the helical angle (Fig. 4(c)) [42,43]. A simple circuit model was also developed to understand the resistance-changing process, in which R_1 is the resistance of the neighboring coils of the silver-plated nylon yarn, and R_c refers to the resistance of the stapled fibers from the twisted structure. The increased distance between the gapped silver-plated fibers is expected to decrease the conductive capability, thereby causing an increase in the resistance of each contact area [44]. In our cyclical stretching/releasing experiment, HCSY was exposed to a strain of 50% for over 15 000 tensile cycles (Fig. 4(d)), during which the resistance change was nearly constant and the hysteresis of the basic resistance was only 5.36%. The irreversible change in resistance can be attributed primarily to the viscoelastic properties of the elastic yarns and the incoherent deformations occurring between the wrapped silver-plated nylon, which result in interconnect damage and internal wire slippage. Fig. S16 in Appendix A illustrates the resistance evolution during cyclic stretching following exposure to the chemical solution. The results indicate the excellent sensing stability of the HCSY after undergoing the chemical resistance test. This can be attributed to the surface-structured PTFE protective layers, a barrier in constructing anti-chemical protective suits. Fig. S17 in Appendix A illustrates that the resistance signal of the HCSY gradually increases with increasing spiral angles and bending distances when the sensor is subjected to torsion and bending. Notably, the 10 cm long HCSY device demonstrated remarkable and consistent sensing properties across various strains, frequencies, and relative humidities, as depicted in Appendix A Fig. S18. The adaptivity of the sensor is crucial in wearable applications as it ensures a reliable response to different external stimuli, thus guaranteeing the sensor's overall reliability.

3.4. Human–machine interaction of HCSY

Real-time monitoring of human physiological signals in extreme environments is crucial for chemical protective suits [12,15,37,43]. These include motions associated with walking, shaking the beaker, or formulating chemical reagents (Figs. 5(a)–(c) and Fig. S19 in Appendix A). These results confirm the exceptional strain-sensing performance of the HCSY, thus ensuring their suitability as wearable devices for detecting various human physiological activities. More importantly, this electrically responsive HCSY can remotely operate a manipulator after it is connected to a series circuit to prevent safety hazards in extreme environments [45–47]. Herein, we demonstrated the collective application of five HCSY sensors as a practical wearable sensor platform in a human–machine interface. The strain sensors were sewn onto the surface of five knuckles of a glove. The real-time relative resistance change signal was generated as the finger was bent, and the recognition result was obtained with an accuracy of 94.16% (Figs. 5(d) and (e)) after 1000 iterations of training and testing using the *K*-nearest neighbor (KNN) model. Based on the high-precision gesture recognition function, the corresponding fingers of the manipulator received the changing signal and quickly repeated the same action when the human forefinger was bent, whereas the other parts remained still, as shown in Fig. 5(f). The five fingers of the manipulator and the corresponding five human fingers bent simultaneously, thereby allowing for a high-sensitivity grip on either a beaker or a pipette gun (Movie S3 in Appendix A). Therefore, the HCSY has broad application potential in controlling

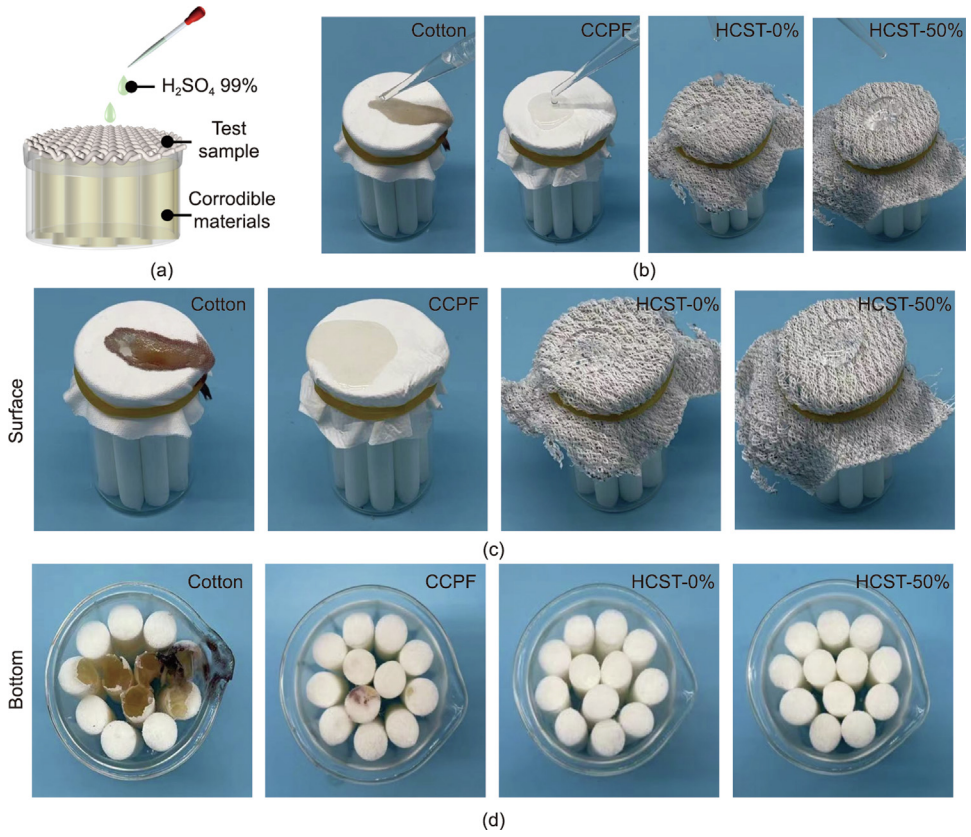

Fig. 3. Chemical resistance characterization of HCST. (a) Schematic of self-built chemical resistance test device. (b) Optical images of the sample surface after dipping by 1 mL of 99 wt% H_2SO_4. (c) Optical images of the sample surface after being exposed to 99 wt% H_2SO_4 for 10 min. (d) Optical images of the corrodible materials after removing the covered fabrics.

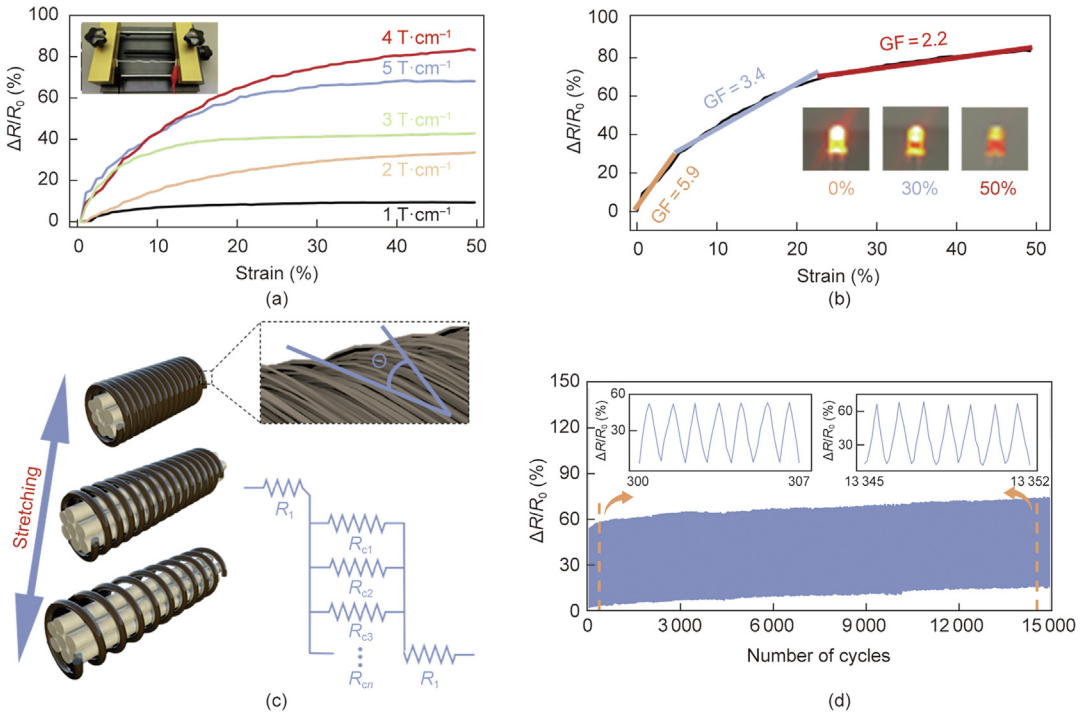

Fig. 4. Strain sensing performance of HCSY. (a) $\Delta R/R_0$ change as a function of strain for HCSY at different wrapping twists. (b) $\Delta R/R_0$ of HCSY versus the applied strain (wrapping twists 4 T·cm^{-1}, and the HCSY sensor is 10 cm long.). (c) Schematic of the proposed mechanism of HCSY based on helical conductive conformational changes at different states and a proposed schematic resistance model of an elementary unit. (d) $\Delta R/R_0$ variation of HCSY at repeated stretch/release cycles with a 50% strain. Inserted pictures show real-time capacitive change of HCSY at position of orange dotted line.

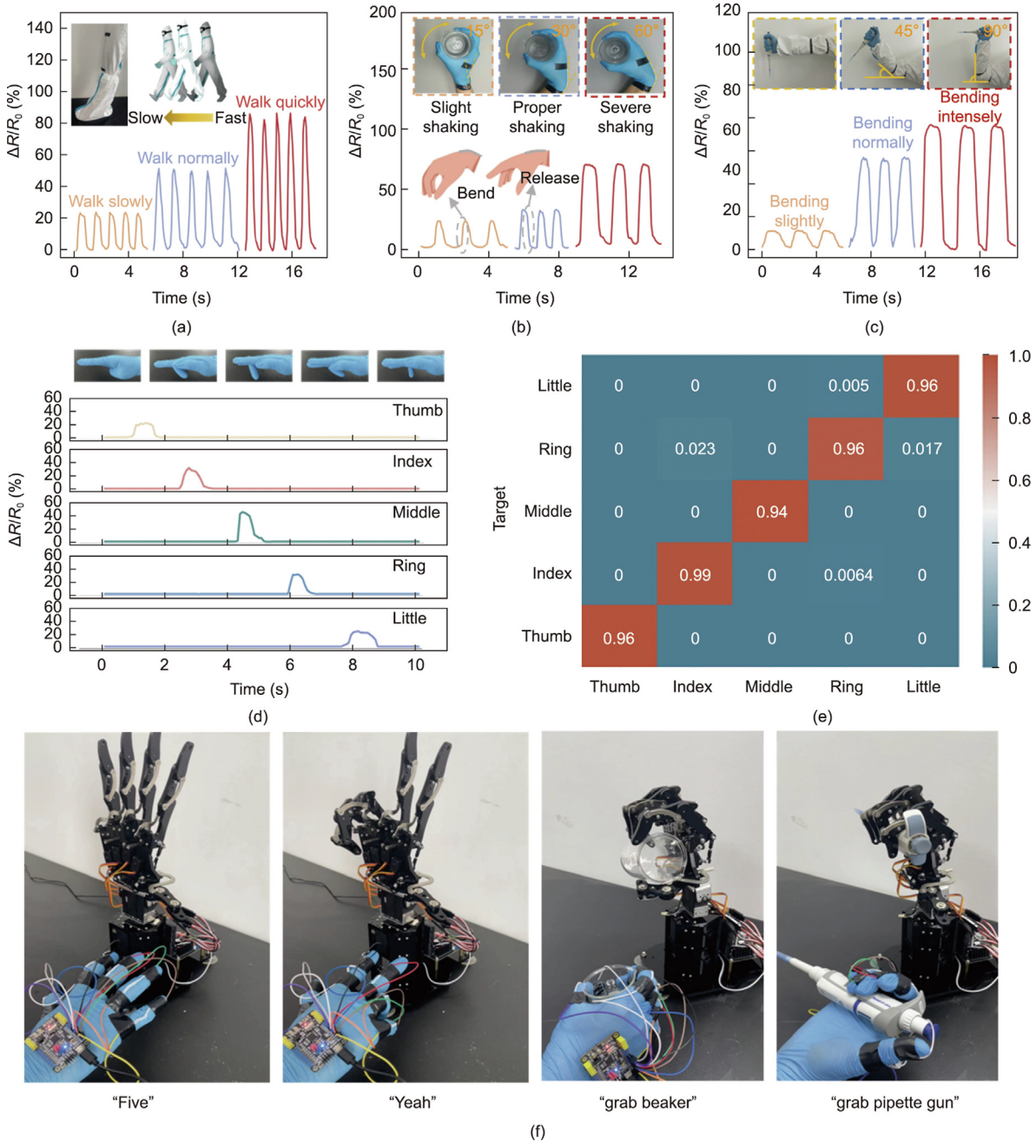

Fig. 5. Human–machine interaction performance of HCSYs. Strain sensing detection of human motions by integrated HCSYs onto a CCPS and the corresponding response signals to (a) bending of the knee joint, (b) flexion and rotation of the wrist, and (c) bending of the elbow. The inserted photographs show an HCSY device attached to (a) the knee joint bent at different frequencies for walking motion, (b) wrist flexed and rotated at different angles in different shaking ranges, and (c) elbow bent at different angles for chemical solution preparation. (d) Using the generated signals from five fingers to monitor various hand gestures. (e) KNN model showing the classification accuracies (%) of the different hand gestures. (f) Real-time demonstration of the human–machine remote control system for synchronized operations in high-risk environments.

instruments by monitoring the movement of human limbs when facing potential chemical dangers.

3.5. Tunable thermoregulation function and thermal management of HCSTs

The thermal management of functional textiles has gained considerable importance in ensuring wearable comfort [29,47,48]. The excellent tensile properties of HCSTs provide not only stretchable sensing performance but also enable adjustable thermoregulation functions. First, we conducted measurements on the air and water vapor permeabilities of HCST pieces to confirm their tunable thermal and moisture management capabilities. At a strain of 50%, the presence of separating domains within the gapped PTFE layer facilitated the easy flow of gas and water molecules, thus leading to higher air permeability and water vapor transmission in the HCST (Fig. 6(a)). In addition, we examined the thermal resistance of HCSTs at different strain levels. The results revealed that the HCSTs exhibited adjustable thermal conductivity (Fig. 6(b)). As shown in the inserted photograph of Fig. 6(b), Fig. S20, and Movie S4 in Appendix A, the working mechanism of the HCSTs relies on the dynamic formation of thermally conductive interfaces and inter yarn spaces upon mechanical actuation. Consequently, implementing a hierarchical structural design facilitates the

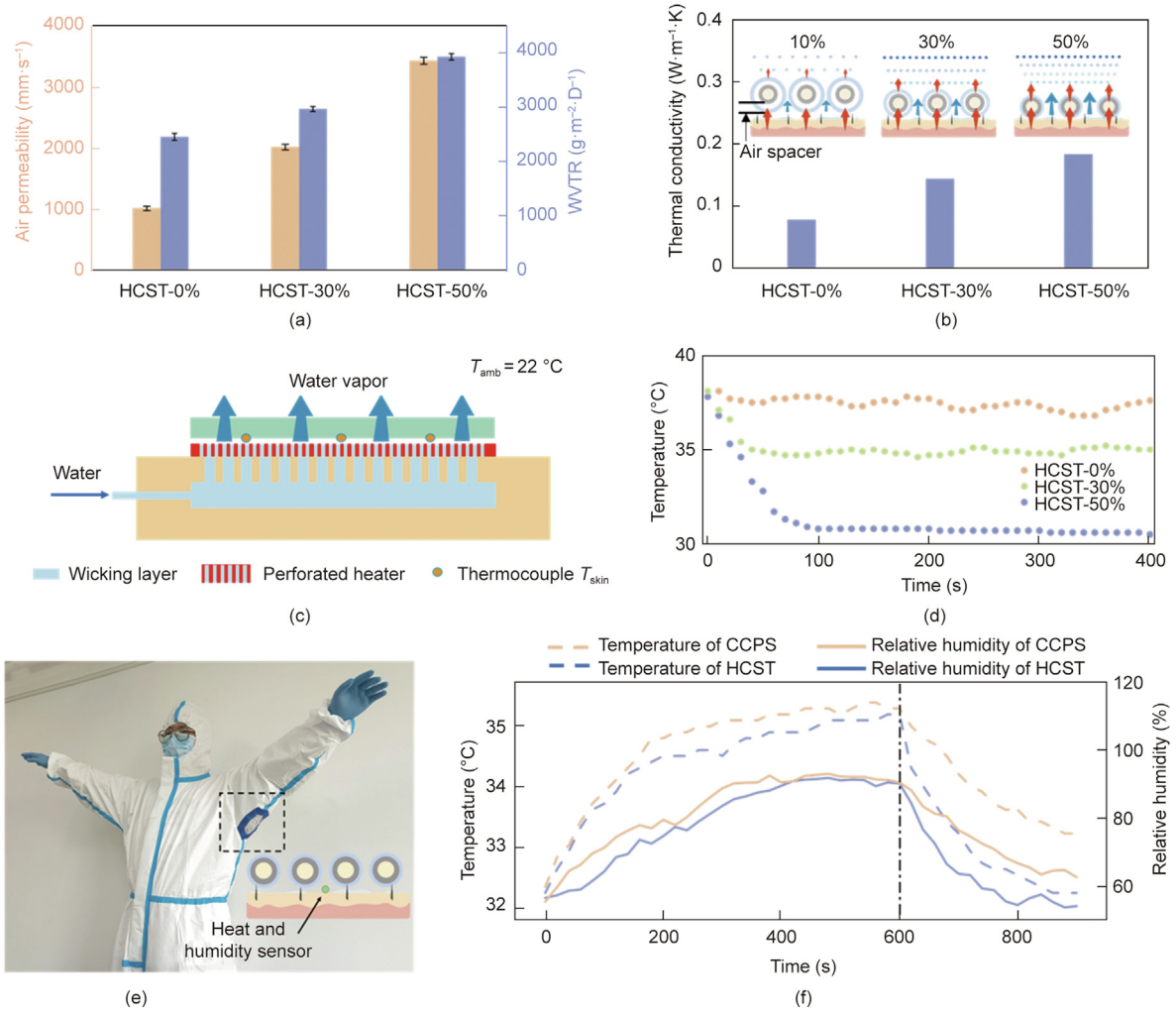

Fig. 6. Tunable thermoregulation function of HCST. (a) Air permeability and moisture permeability of HCSTs at different strain ratios (10%, 30%, and 50%). WVTR: water vapor transmission rate. (b) Thermal conductivity of HCSTs at different strain ratios (10%, 30%, and 50%) at 25 °C. The inserted photographs show the working mechanisms of our HCSTs interacting with adjustable thermal conductive interfaces and separating domains with different mechanical actuation. (c) Schematic of the tunable thermal management test. T_{amb}: ambient temperature, T_{skin}: skin temperature. (d) Lower part temperatures of HCSTs at different strain ratios were measured by the thermocouple in a purpose-designed experimental environment. (e) Photograph of a person wearing a chemical protective suit with an integrated piece of HCST. (f) Comparison of the as-measured temperature and humidity of a person wearing a CCPS with and without HCST integration during exercising and releasing states.

efficient transfer of heat from the human body to the surrounding environment [49]. Herein, the cooling performance of HCSTs at different strains was compared based on a purpose-designed experimental setup (Fig. 6(c)), in which artificial sweat was added continuously at 37.6 °C at a rate of 100 μL·min^{-1} onto the artificial skin and power density of the artificial skin was maintained constant at the temperature of 37.6 °C (power density, 80 W·m^{-2}). The prewet artificial skin was covered with various fabric samples to monitor and record the near-skin temperature. As sweat evaporated and heat dissipated, the skin temperature steadily decreased. The near-skin temperature with HCSTs changed from 37.6 to 31.2 °C after the application of 50% strain (Fig. 6(d)), thus demonstrating that the human body can effectively evaporate sweat and dissipate body heat to achieve lower skin temperatures owing to its functional, structural design [40–52]. After contact with H_2SO_4 for 10 min, hardly any decrease in thermoregulatory function was observed (Fig. S21 in Appendix A), possibly because the braided PTFE protective layer effectively blocked chemical penetration and maintained gapped domain control. Thus, even after undergoing chemical treatment, the thermal management of the HCSYs remains uncompromised.

To test the actual wearing performance of the tunable heat management, a piece of HCST was sewn into the underarm of a CCPS and examined at 28 °C and 62% humidity (Fig. 6(e)). Additionally, a heat–humidity sensor was placed near the underarm area to monitor near-skin temperature and humidity changes. During strenuous exercise, when the HCST piece was slightly stretched, the rate of increase in near-skin temperature and humidity, as measured by the individual wearing the protective clothing integrated with HCSTs, was slightly lower than that of the CCPS. After 600 s, the HCST was fully stretched when the participant stood with raised arms to dissipate heat. Compared with the value of CCPS after 900 s, the temperature at the HCST was approximately 1.1 °C lower, and the humidity was reduced by 7.6% (Fig. 6(f)), thus clearly demonstrating the effectiveness of the thermoregulation function of HCSTs.

The synergistic effects observed were chemical resistance of the braided–structured PTFE protective layers from the outer layer, stretch-introduced resistance sensing of helically wrapped silver-plated nylon yarns from the inner layer, and dynamic thermoregulation of the strain-reconfigurable structure from the hierarchical functional design in the HCSYs. Consequently, the desired HCSYs/

HCSTs can effectively overcome the trade-off between chemical harm protection, real-time motion detection, and adjustable heat diffusion. This integration allows superior chemical protection, strain sensing, and thermal management capabilities.

4. Conclusions

Herein, we proposed a multifunctional intelligent yarn and fabric featuring unique hierarchical core–shell structures. These structures can be created through continuous and large-scale fabrication processes. The outcomes of our research contribute to an innovative chemical hazard protection textile. This textile combines real-time motion detection and adjustable heat management properties. The hierarchical structural design of the helically wrapped silver-plated nylon sensing layer resulted in electrical signal variations, which were utilized for monitoring human motion, essentially offering outstanding sensitivity, stability, and durability. Furthermore, the HCST includes a surface-structured PTFE protective layer, which addresses acid and alkali resistance, and provides user-tunable thermoregulability properties from the stretching-induced variations in yarn spacing. Therefore, durable, flexible, and scalable smart protective yarns with hierarchical core–shell structures can be efficiently manufactured and developed as next-generation chemical protective textiles for use in chemical laboratories, plants, special workshops, and emergency sites.

Declaration of competing interest

The authors declare that they have no known competing financial interests or personal relationships that could have appeared to influence the work reported in this paper.

Acknowledgments

Funding was received from the National Key Research and Development Program of China (2022YFB3805800), the National Natural Science Foundation of China (52173059 and U21A2095), the Postgraduate Research and Practice Innovation Program of Jiangsu Province (KYCX223203), the Major Basic Research Project of the Natural Science Foundation of the Jiangsu Higher Education Institutions (21KJA540002), and the Key Research and Development Program of Hubei Province (2021BAA068).

Compliance with ethics guidelines

Duo Xu, Yingcun Liu, Can Ge, Chong Gao, Ze Chen, Ziyi Su, Haoran Gong, Weilin Xu, and Jian Fang declare that they have no conflict of interest or financial conflicts to disclose.

Appendix A. Supplementary material

Supplementary data to this article can be found online at https://doi.org/10.1016/j.eng.2023.06.018.

References

[1] Bhattacharjee S, Joshi R, Chughtai AA, Macintyre CR. Graphene modified multifunctional personal protective clothing. Adv Mater Interfaces 2019;6(21):1900622.
[2] Shi J, Li H, Xu F, Tao X. Materials in advanced design of personal protective equipment: a review. Mater Today Adv 2021;12:100171.
[3] Ma L, Wu R, Patil A, Yi J, Liu D, Fan X, et al. Acid and alkali-resistant textile triboelectric nanogenerator as a smart protective suit for liquid energy harvesting and self-powered monitoring in high-risk environments. Adv Funct Mater 2021;31(35):2102963.
[4] Karim N, Afroj S, Lloyd K, Oaten LC, Andreeva DV, Carr C, et al. Sustainable personal protective clothing for healthcare applications: a review. ACS Nano 2020;14(10):12313–40.
[5] Singh N, Tang Y, Ogunseitan OA. Environmentally sustainable management of used personal protective equipment. Environ Sci Technol 2020;54(14):8500–2.
[6] Wu R, Ma L, Hou C, Meng Z, Guo W, Yu W, et al. Silk composite electronic textile sensor for high space precision 2D combo temperature–pressure sensing. Small 2019;15(31):e1901558.
[7] Alagumalai A, Shou W, Mahian O, Aghbashlo M, Tabatabaei M, Wongwises S, et al. Self-powered sensing systems with learning capability. Joule 2022;6(7):1475–500.
[8] Niu H, Li H, Gao S, Li Y, Wei X, Chen Y, et al. Perception-to-cognition tactile sensing based on artificial-intelligence-motivated human full-skin bionic electronic skin. Adv Mater 2022;34(31):e2202622.
[9] Lu W, Yu P, Jian M, Wang H, Wang H, Liang X, et al. Molybdenum disulfide nanosheets aligned vertically on carbonized silk fabric as smart textile for wearable pressure-sensing and energy devices. ACS Appl Mater Interfaces 2020;12(10):11825–32.
[10] Lipomi DJ, Vosgueritchian M, Tee BC, Hellstrom SL, Lee JA, Fox CH, et al. Skin-like pressure and strain sensors based on transparent elastic films of carbon nanotubes. Nat Nanotechnol 2011;6(12):788–92.
[11] Shi J, Liu S, Zhang L, Yang B, Shu L, Yang Y, et al. Smart textile-integrated microelectronic systems for wearable applications. Adv Mater 2020;32(5):e190195.
[12] Busolo T, Szewczyk PK, Nair M, Stachewicz U, Kar-Narayan S. Triboelectric yarns with electrospun functional polymer coatings for highly durable and washable smart textile applications. ACS Appl Mater Interfaces 2021;13(14):16876–86.
[13] Zhao H, Zhou Y, Cao S, Wang Y, Zhang J, Feng S, et al. Ultrastretchable and washable conductive microtextiles by coassembly of silver nanowires and elastomeric microfibers for epidermal human–machine interfaces. ACS Materials Lett 2021;3(7):912–20.
[14] Wang R, Du Z, Xia Z, Liu J, Li P, Wu Z, et al. Magnetoelectrical clothing generator for high-performance transduction from biomechanical energy to electricity. Adv Funct Mater 2022;32(6):2107682.
[15] Fu C, Wang K, Tang W, Nilghaz A, Hurren C, Wang X, et al. Multi-sensorized pneumatic artificial muscle yarns. Chem Eng J 2022;446:137241.
[16] Song J, Tan Y, Chu Z, Xiao M, Li G, Jiang Z, et al. Hierarchical reduced graphene oxide ridges for stretchable, wearable, and washable strain sensors. ACS Appl Mater Interfaces 2019;11(1):1283–93.
[17] Li Y, Zhang Y, Yi J, Peng X, Cheng R, Ning C, et al. Large-scale fabrication of core-shell triboelectric braided fibers and power textiles for energy harvesting and plantar pressure monitoring. EcoMat 2022;4(4):e12191.
[18] Liu M, Pu X, Jiang C, Liu T, Huang X, Chen L, et al. Large-area all-textile pressure sensors for monitoring human motion and physiological signals. Adv Mater 2017;29(41):1703700.
[19] Zhu C, Wu J, Yan J, Liu X. Advanced fiber materials for wearable electronics. Adv Fiber Mater 2023;5(1):12–35.
[20] Gan L, Zeng Z, Lu H, Li D, Wei K, Cai G, et al. A large-scalable spraying–spinning process for multifunctional electronic yarns. SmartMat 2023;4(2):e1151.
[21] Du X, Tian M, Sun G, Li Z, Qi X, Zhao H, et al. Self-powered and self-sensing energy textile system for flexible wearable applications. ACS Appl Mater Interfaces 2020;12(50):55876–83.
[22] Huang F, Wei Q, Liu Y, Gao W, Huang Y. Surface functionalization of silk fabric by PTFE sputter coating. J Mater Sci 2007;42(19):8025–8.
[23] Luo J, Gao S, Luo H, Wang L, Huang X, Guo Z, et al. Superhydrophobic and breathable smart MXene-based textile for multifunctional wearable sensing electronics. Chem Eng J 2021;406:126898.
[24] Wen F, Sun Z, He T, Shi Q, Zhu M, Zhang Z, et al. Machine learning glove using self-powered conductive superhydrophobic triboelectric textile for gesture recognition in VR/AR applications. Adv Sci 2020;7(14):2000261.
[25] Lu D, Liao S, Chu Y, Cai Y, Wei Q, Chen K, et al. Smart highly durable and fast response fabric strain sensor for movement monitoring under extreme conditions. Adv Fiber Mater 2023;5(1):223–34.
[26] Dong J, Wei Q, Wang D, Peng Y, Zhang C, Lai F, et al. Surface ultra-stretchable and superhydrophobic textile-based bioelectrodes for robust self-cleaning and personal health monitoring. Nano Energy 2022;97:107160.
[27] Bloomfield EL. Prolonged wear of antichemical protective gear: the hazards and difficulties of wearing chemical warfare gear. Anesthesiology 2004;101(6):1478.
[28] Zeng S, Pian S, Su M, Wang Z, Wu M, Liu X, et al. Hierarchical-morphology metafabric for scalable passive daytime radiative cooling. Science 2021;373(6555):692–766.
[29] Peng Y, Li W, Liu B, Jin W, Schaadt J, Tang J, et al. Integrated cooling (i-Cool) textile of heat conduction and sweat transportation for personal perspiration management. Nat Commun 2021;12(1):6122.
[30] Trung TQ, Le HS, Dang TML, Ju S, Park SY, Lee NE. Freestanding, fiber-based, wearable temperature sensor with tunable thermal index for healthcare monitoring. Adv Healthc Mater 2018;7(12):e1800074.
[31] Wang H, Zhang Y, Liang X, Zhang Y. Smart fibers and textiles for personal health management. ACS Nano 2021;15(8):12497–508.
[32] Lu D, Liao S, Chu Y, Cai Y, Wei Q, Chen K, et al. Highly durable and fast response fabric strain sensor for movement monitoring under extreme conditions. Adv Fiber Mater 2023;5(1):223–34.

[33] National Bureau of Technical Supervision. GB/T 5453-1997: Textiles-determination of the permeability of fabrics to air. Chinese standard. Beijing: National Standards of the People's Republic of China; 1997. Chinese.
[34] ASTM E398; Standard test method for water vapor transmission rate of sheet materials using dynamic relative humidity measurement. ASTM standard. Philadelphia: American Society of Testing Materials; 2003.
[35] ISO 22007–2: Plastics—determination of thermal conductivity and thermal diffusivity—part 2: transient plane heat source (hot disc) method. ISO standard. Geneva: International Organization for Standardization; 2008.
[36] Wu R, Seo S, Ma L, Bae J, Kim T. Full-fiber auxetic-interlaced yarn sensor for sign-language translation glove assisted by artificial neural network. Nano-Mirco Lett 2022;14:139.
[37] Zhang Q, Wang Y, Xia Y, Zhang P, Kirk T, Chen X. Textile-only capacitive sensors for facile fabric integration without compromise of wearability. Adv Mater Technol 2019;4(10):1900485.
[38] Cai G, Yang M, Pan J, Cheng D, Xia Z, Wang X, et al. Large-scale production of highly stretchable CNT/cotton/spandex composite yarn for wearable applications. ACS Appl Mater Interfaces 2018;10(38):32726–35.
[39] Cai G, Hao B, Luo L, Deng Z, Zhang R, Ran J, et al. Highly stretchable sheath–core yarns for multifunctional wearable electronics. ACS Appl Mater Interfaces 2020;12(26):29717–27.
[40] Zeng Z, Hao B, Li D, Cheng D, Cai G, Wang X. Large-scale production of weavable, dyeable and durable spandex/CNT/cotton core–sheath yarn for wearable strain sensors. Compos Part A Appl Sci 2021;149:106520.
[41] Wu J, Wang Z, Liu W, Wang L, Xu F. Bioinspired superelastic electroconductive fiber for wearable electronics. ACS Appl Mater Interfaces 2019;11 (47):44735–41.
[42] Yang M, Fu C, Xia Z, Cheng D, Cai G, Tang B, et al. Conductive and durable CNT-cotton ring spun yarns. Cellul 2018;25(7):4239–49.
[43] Zhang Y, Li T, Shiu B, Lin J, Lou C. Multifunctional sodium alginate@ urushiol fiber with targeted antibacterial, acid corrosion resistance and flame retardant properties for personal protection based on wet spinning. Appl Surf Sci 2022;584:152573.
[44] Qu X, Wu Y, Ji P, Wang B, Liang Q, Han Z, et al. Crack-based core–sheath fiber strain sensors with an ultralow detection limit and an ultrawide working range. ACS Appl Mater Interfaces 2022;14(25):29167–75.
[45] Shen Z, Zhang Z, Zhang N, Li J, Zhou P, Hu F, et al. High-stretchability, ultralow-hysteresis conducting polymer hydrogel strain sensors for soft machines. Adv Mater 2022;34(32):e2203650.
[46] Schwartz G, Tee BC, Mei J, Appleton AL, Kim DH, Wang H, et al. Flexible polymer transistors with high pressure sensitivity for application in electronic skin and health monitoring. Nat Commun 2013;4(1):1859.
[47] Badshah M, Leung E, Liu P, Strzelecka A, Gorodetsky A. Scalable manufacturing of sustainable packaging materials with tunable thermoregulability. Nat Sustain 2022;5(5):434–43.
[48] Lao L, Shou D, Wu YS, Fan JT. "Skin-like" fabric for personal moisture management. Sci Adv 2020;6(14):eaaz0013.
[49] Cai L, Peng Y, Xu J, Zhou C, Zhou C, Wu P, et al. Temperature regulation in colored infrared-transparent polyethylene textiles. Joule 2019;3(6):1478–86.
[50] Zhang X, Yang W, Shao Z, Li Y, Su Y, Zhang Q, et al. A moisture-wicking passive radiative cooling hierarchical metafabric. ACS Nano 2022;16(2):2188–97.
[51] Fu K, Yang Z, Pei Y, Wang Y, Xu B, Wang Y, et al. Designing textile architectures for high energy–efficiency human body sweat- and cooling-management. Adv Fiber Mater 2019;1(1):61–70.
[52] Peng Y, Lee H, Wu D, Cui Y. Bifunctional asymmetric fabric with tailored thermal conduction and radiation for personal cooling and warming. Engineering 2022;10:167–73.